Available online at www.sciencedirect.com
SCIENCE DIRECT®
Journal of Photochemistry and Photobiology A: Chemistry 163 (2004) 281–287
Journal of Photochemistry and Photobiology A:Chemistry
www.elsevier.com/locate/jphotochem

Photodegradation of dye pollutants on silica gel supported TiO_2 particles under visible light irradiation

Yingxu Chen*, Kan Wang, Liping Lou

Department of Environmental Engineering, Zhejiang University, Hangzhou 310029, PR China

Received 8 September 2003; received in revised form 25 November 2003; accepted 22 December 2003

Abstract

In this paper, silica gel supported titanium dioxide particles (TiO_2/SiO_2) prepared by acid-catalyzed sol–gel method was as photocatalyst in the degradation of acid orange 7 (AO7) in water under visible light irradiation. The particles were characterized by X-ray diffraction, BET specific surface area determination, and point of zero charge measurement. The supported catalyst had large surface area, high thermal stability and good sedimentation ability. The photodegradation rate of AO7 under visible light irradiation depended strongly on adsorption capacity of the catalyst, and the photoactivity of the supported catalyst was much higher than that of the pure titanium dioxides. The photodegradation rate of AO7 using 31% TiO_2/SiO_2 particles was faster than that using P-25 and TiO_2 (Shanghai) as photocatalyst by 2.3 and 12.3 times, respectively. The effect of the calcination temperature and the TiO_2 loading on the photoactivity of TiO_2/SiO_2 particles was also discussed.

Keywords: TiO_2; Silica gel; Photodegradation; Visible light; Dye pollutants

1. Introduction

Dye pollutants produced from the textile industries are becoming a major source of environmental contaminations [1]. It is estimated that about 15% of the total world production of dyes is lost during the dyeing and finishing operations and is released in the textile effluents [2]. Azo dyes, which contain one or more nitrogen to nitrogen double bonds (–N=N–) and constitute a significant portion of dye colorants, are widely used in the dyeing industry today, and are also resistant to aerobic degradation and under anaerobic conditions they can be reduced to potentially carcinogenic aromatic amines [3–5].

For the treatment of dye-containing wastewater, traditional methods such as flocculation, carbon adsorption, reverse osmosis and activated sludge process has difficulties in the complete destruction of dye pollutants [6], and has the further disadvantage of potentially secondary pollution [7]. So in recent years, heterogeneous photocatalytic oxidation has received considerable attention for the destructive oxidation of dyes and textile effluents, since many aromatic compounds have proven to be degraded effectively to CO_2, H_2O and small molecules [8–10]. Among the various photocatalysts employed, TiO_2 is the most preferable material due to its non-toxic, insoluble, stability, high photoactivity and inexpensive nature. However, TiO_2 can only utilize a relative small part (less than 5%) of the solar spectrum for photocatalytic oxidation and artificial UV light sources are unstable and expensive, which are main barriers to marketing the TiO_2 photocatalytic oxidation processes. Moreover, most of commercial TiO_2 usually have small particle sizes so that TiO_2 particles are difficult to recovery from the suspension, such as by filtration.

Early studies reported that a dye molecule in its exited state generated upon visible light irradiation can transfer an electron to the conduction band of semiconductor particles [11–14], which provide a new method for the treatment or pre-treatment of dye-containing wastewater. The mechanism of dye degradation under visible light irradiation is described by Eqs. (1)–(6) [15]:

$$\text{dye} + h\upsilon \rightarrow \text{dye}^* \quad (1)$$

$$\text{dye}^* + \text{TiO}_2 \rightarrow \text{dye}^{\bullet+} + \text{TiO}_2(\text{e}) \quad (2)$$

$$\text{TiO}_2(\text{e}) + \text{O}_2 \rightarrow \text{TiO}_2 + \text{O}_2^{\bullet-} \quad (3)$$

$$\text{O}_2^{\bullet-} + \text{TiO}_2(\text{e}) + 2\text{H}^+ \rightarrow \text{H}_2\text{O}_2 \quad (4)$$

* Corresponding author. Tel.: +86-571-86971159; fax: +86-571-86971898.
E-mail addresses: yxchen@zju.edu.cn (Y. Chen), wangkan@zju.edu.cn (K. Wang).

1010-6030/$ – see front matter © 2004 Elsevier B.V. All rights reserved.
doi:10.1016/j.jphotochem.2003.12.012

$$H_2O_2 + TiO_2(e) \rightarrow {}^{\bullet}OH + OH^- \quad (5)$$

$$dye^{\bullet+} + O_2(\text{or } O_2{}^{\bullet-} \text{ or } {}^{\bullet}OH) \rightarrow \text{peroxylated or hydroxylated intermediates} \rightarrow\rightarrow \text{degraded or mineralized products} \quad (6)$$

Therefore, the mechanism of dye degradation under visible light illumination is different from the UV irradiation pathway, where dyes rather than TiO_2 particles are excited by visible light.

On the other hand, since one of the important criteria for an efficient photosensitization is to adsorb the dye on the TiO_2 surface and photodegradation reaction under visible light irradiation only takes place on the TiO_2 surface, large surface area and high adsorption capacity are very important to increase the photoactivity of TiO_2 particles. A feasible approach to achieve these things is the use of adsorbents with large surface area as supporting materials for TiO_2 loading.

In this paper, silica gel was selected as support for TiO_2 loading. A series of TiO_2/SiO_2 were prepared under different conditions to investigate the effect of the TiO_2 loading and the calcination temperature on the photoactivity of the catalysts. Characterization of TiO_2/SiO_2 photocatalysts was reported employing powder X-ray diffraction (XRD), BET specific surface area determination, and point of zero charge measurement. Photoactivity of the catalysts was evaluated using the photodegradation of an azo-dye acid orange 7 (AO7) under visible light irradiation.

2. Experimental

2.1. Materials

Acid orange 7 was obtained from Sigma and was used without further purification. TiO_2 P-25 (ca. 80% anatase, 20% rutile; BET area, ca. 50 $m^2\,g^{-1}$; mean particle size, ca. 30 nm) was supplied by Degussa Co. TiO_2 (Shanghai, average particles size as measured by SEM about 0.95 μm, mainly of anatase form conformed by XRD, BET area, ca. 11 $m^2\,g^{-1}$) was obtained from Shanghai Chemical Company. Silica gel (100–200 mesh) was obtained from Shanghai Chemical Company. All other chemicals were of analytical reagent grade quality and were employed without further purification. All experiments were carried out using deionized and double distilled water. The pH of the solution was adjusted with either diluted HNO_3 or NaOH. The structure of the AO7 molecule is illustrated in Fig. 1.

2.2. Preparation of supported TiO_2 photocatalysts

The TiO_2 sol was synthesized by the method called acid-catalyzed sol–gel process. A typical procedure was as follows: Tetrabutyl titanate of 8.5 ml was added to 30 ml and 1 M HNO_3 aqueous solution, stirring at the same time, followed by agitation for 1 h and a flaxen transparent TiO_2 sol was obtained. Then, the solution was diluted by adding distilled water of 60 ml. The pH of the solution was adjusted to 2 using 1 M NaOH, followed by stirring for 1 h to give a turbid TiO_2 colloid. A certain amount of silica gel was added to the TiO_2 colloid, with stirring for 1 h, and then followed by adjusting pH to 3. The suspension was stirring for 1 h, followed by washing-centrifugation procedure to make the supernatant nearly neutral. Then the supported TiO_2 particles was dried at 70 °C for 24 h and calcined at different temperatures for 2 h.

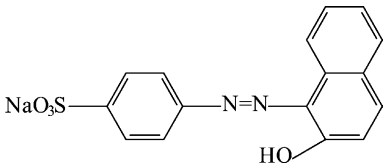

Fig. 1. The structure of the AO7 molecule.

2.3. Chemical analysis of titanium oxide

The amount of TiO_2 loading of supported TiO_2 particles (TiO_2/SiO_2) was determined by colorimetric analysis using H_2O_2 as a complex agent [16]. In this paper, the silica gel supported particles was denoted as *x*% TiO_2/SiO_2, where *x*% was the amount of TiO_2 loading by weight.

2.4. Photocatalytic experiments

The experiments were performed in a Pyrex reactor of 1000 ml capacity. A 175 W metal halide lamp (Philips) was used as the light source and positioned inside a cylindrical vessel surrounded by a jacket. $NaNO_2$ solutions (2 M) were circulated through the jacket to filter out the UV emission of the lamp below 400 nm and cool the reactor to 20 °C. In a typical experiment, a certain amount of AO7 was dissolved in 1000 ml of distilled water, resulting in a solution with pH 5.7. Prior to irradiation, a suspension containing 2 g of catalyst and 1000 ml of AO7 solution was stirred continuously in the dark for 1 h to achieve the adsorption equilibrium of AO7 on the surface of the catalyst. The concentration of substrate in bulk solution at this point was used as the initial value of the further kinetic treatment of the photodegradation process. All irradiation were carried out under constant stirring. At given intervals of irradiation, a sample of the catalyst particles was collected, centrifuged, and then filtered through a Millipore filter (pore size 0.22 μm). The filtrates were analyzed by UV-Vis spectroscopy using a Shimadzu UV1206 spectrophotometer. The determination wavelength is 484 nm for AO7, which is the maximum absorption wavelength. The determined absorption was converted to concentration through the standard curve of the dye ($r = 0.9999$).

2.5. Characterization

The phase of supported photocatalyst was studied by the powder XRD technique. The patterns were recorded on a Rigaku X-ray diffractometer using Cu Kα radiation. Diffraction patterns were taken over the 2θ range 20–70°. Average crystallite size of prepared particles was calculated by the Scherrer's equation.

The BET specific surface area was determined by nitrogen physisorption data at 77 K using Coulter OMNISORP-100 instrument. Pore volume and pore size distributions were determined by Barrett–Joyner–Halenda (BJH) method with cylindrical geometry of the pores.

The point of zero charge (pzc) of the photocatalyst was measured by the method of mass titration [17,18].

2.6. Kinetics

In general, the influence of initial concentration of organic pollutants on the photodegradation rate has been described well by the Langmuir–Hinshelwood kinetic model (Eq. (7)) [19,20].

$$r = \frac{dC}{dt} = \frac{kKC}{1 + KC} \tag{7}$$

At low substrate concentrations, the above equation can be simplified to a pseudo-first-order equation (Eq. (8)).

$$\ln\left(\frac{C_0}{C}\right) = kKt = k't \tag{8}$$

where r is the oxidation rate of the reactant (mg/l min), C_0 the initial concentration of the reactant (mg/l), C the concentration of the reactant at time t (mg/l), t the irradiation time, k the reaction rate constant (min^{-1}), and K the adsorption coefficient of the reactant onto the semiconductor particles (l/mg).

3. Results and discussion

3.1. Characterization of TiO_2/SiO_2 photocatalyst

3.1.1. XRD analysis

Figs. 2 and 3 show the XRD patterns of TiO_2/SiO_2 particles with different calcination temperatures and TiO_2 loadings, respectively. The peaks corresponding the anatase TiO_2 phase appeared at $2\theta = 25.3$, 37.8, 48.0, 54.4 and 62.8°. As observed in Fig. 2, the major phase of TiO_2/SiO_2 particles at different calcination temperatures was pure anatase. The peaks were getting sharper with increasing the calcination temperature, showing that the average crystallite size increased with increasing the calcination temperature. As shown in Fig. 3, for the catalysts with high TiO_2 loading (>31%), the major phase of the TiO_2/SiO_2 particles was anatase. However, for the catalysts with low TiO_2 loading, the major phase of TiO_2/SiO_2 particles was amorphous, indicating that the high surface area of silica gel helped the dispersion of very fine TiO_2 particles on the support. Moreover, no significant rutile phase was observed for all TiO_2 loadings and calcination temperatures according to the absence of the (1 1 0) rutile reflection at $2\theta \sim 27.4°$, which suggested that the presence of silica gel inhibited the phase transformation of TiO_2 from anatase to rutile. Similar results were also found by Jung and Park [21].

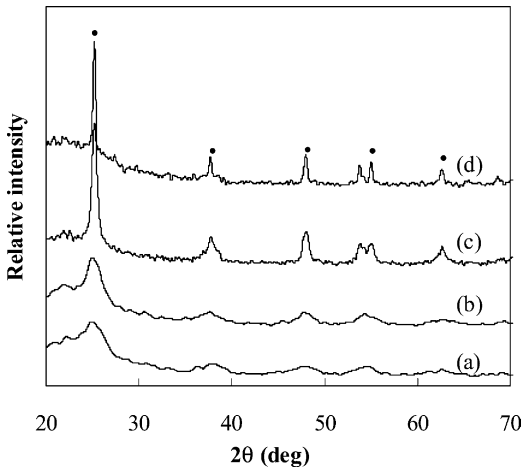

Fig. 2. XRD patterns of TiO_2/SiO_2 particles with the calcination temperature of (a) 70 °C; (b) 300 °C; (c) 500 °C; and (d) 700 °C for 31% TiO_2 loading ((●) labels the diffraction peaks of anatase TiO_2).

The average crystallite sizes of TiO_2 were calculated by Scherrer's equation using the line-width at half-maximum of the X-ray diffraction peaks at $2\theta = 25.3°$ for anatase. Fig. 4 shows the change of the crystallite size of TiO_2/SiO_2 particles with different TiO_2 loadings at the calcination temperature of 300 °C. The average crystallite size of anatase was about 5 nm and increased very slowly with

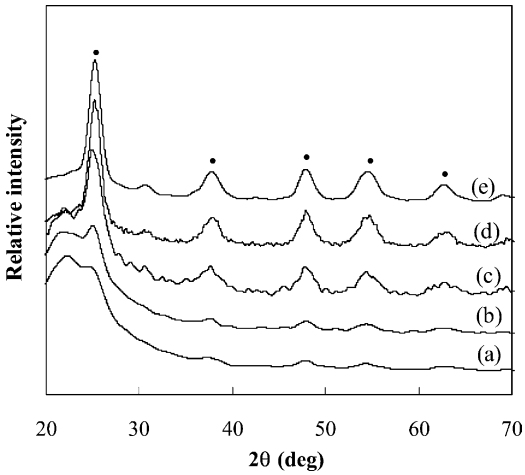

Fig. 3. XRD patterns of TiO_2/SiO_2 particles with the TiO_2 loading of (a) 8%; (b) 18%; (c) 31%; (d) 49%; and (e) 62% at the calcination temperature of 300 °C ((●) labels the diffraction peaks of anatase TiO_2).

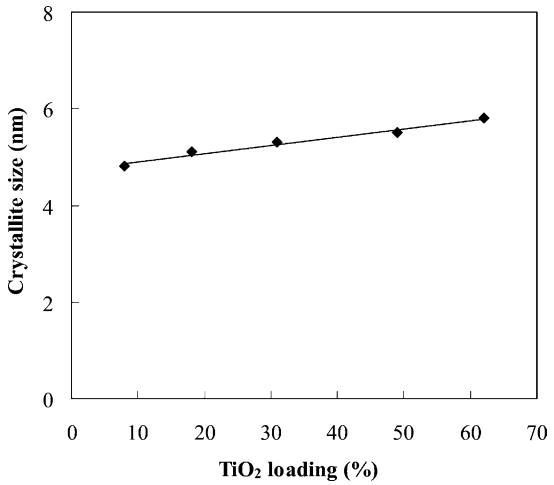

Fig. 4. Crystallite size of the anatase phase of TiO_2/SiO_2 particles as a function of the TiO_2 loading at the calcination temperature of 300 °C.

increasing the TiO_2 loading from 8 to 62%, indicating that the silica gel inhibited the growth of anatase crystal of TiO_2.

3.1.2. BET analysis

Table 1 shows BET surface area, pore volume and average pore size of silica gel before and after it was loaded with TiO_2. The load of TiO_2 decreased BET surface area, pore volume and average pore size of the silica gel. These results indicated that a part of TiO_2 particles dispersed inside the pores of silica gel. As shown in Table 1, BET surface area, pore volume and average pore size of TiO_2/SiO_2 particles were proportionally decreased with increasing the TiO_2 loading. This result was qualitatively reverse with that of the average crystallite size of TiO_2/SiO_2 particles. However, TiO_2/SiO_2 particles retained relatively large surface area and mesopores structure, compared with the P-25 photocatalyst.

BET surface area of 31% TiO_2/SiO_2 particles is shown in Fig. 5 as a function of the calcination temperature. BET surface area was continuously decreased as the calcination temperature increased. It should be noted that the decrease of the surface area of TiO_2/SiO_2 particles was rather slowly, also indicated that the TiO_2 particles was dispersed well on the surface of the silica gel.

Table 1
BET surface area, pore volume and average pore size of the samples

Sample[a]	BET (m^2/g)	Pore volume (cm^3/g)	Average pore size (nm)
Silica gel	347	0.78	9.6
8% TiO_2/SiO_2	272	0.55	8.1
18% TiO_2/SiO_2	254	0.46	7.2
31% TiO_2/SiO_2	225	0.38	6.8
49% TiO_2/SiO_2	214	0.33	6.2
62% TiO_2/SiO_2	194	0.25	5.2

[a] All samples were calcined at 300 °C for 2 h.

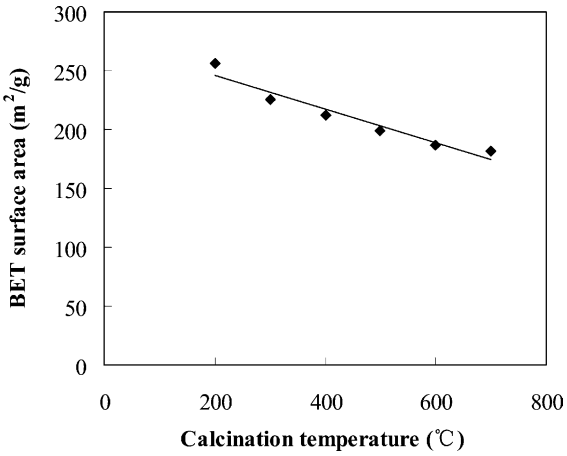

Fig. 5. BET surface area of 31% TiO_2/SiO_2 particles as a function of the calcination temperature.

3.1.3. Point of zero charge measurement

The point of zero charge of TiO_2/SiO_2 particles was measured by using the method of mass titration [17,18]. The pH of the aqueous suspension of oxide depends on the amount of oxide in a given volume of water and the suspension pH often reaches a steady value after addition of excess oxide. This limiting pH is found to be a reasonable estimated for the point of zero charge of each oxide. The pzc value is a useful indicator of the surface acidity of the oxide, which plays an important role in determining adsorption properties of the oxide. In solution of $pH > pH_{pzc}$, the solid surface will be negatively charged, which favors adsorption of cationic ions.

In the case of Degussa P-25, the pzc value estimated by mass titration is 6.1 pH units, while the pzc value of P-25 was 6.25 pH units reported in literature [22]. The differences of the pzc value between literature and present work can be due to specific adsorption of ions or to be the presence of significant amounts of impurities on the surface of TiO_2 particles [18], which lead to a change of the pzc value.

Results of the pzc value of 31% TiO_2/SiO_2 particles under different calcination temperatures are listed in Table 2. As shown in Table 2, the pzc value of 31% TiO_2/SiO_2 particles increased with increasing the calcination temperature, indicating the decomposition of the acidic groups. Table 3 shows the pzc value of TiO_2/SiO_2 particles under different TiO_2 loadings at the calcination temperature of 300 °C. The pzc value of TiO_2/SiO_2 decreased continuously with increasing the TiO_2 loading, and get through a minimum at 31% of the

Table 2
The pzc value of 31% TiO_2/SiO_2 particles under different calcination temperatures

	Calcination temperature (°C)					
	200	300	400	500	600	700
pzc (pH)	2.28	2.66	4.68	4.82	5.06	5.18

Table 3
The pzc value of TiO_2/SiO_2 particles under different TiO_2 loadings at the calcination temperature of 300 °C

	TiO_2 loading (%)				
	8	18	31	49	62
pzc (pH)	3.46	2.88	2.66	2.87	3.04

TiO_2 loading and then increased with increasing the TiO_2 loading, indicating that the effect of the TiO_2 loading on the pzc value of TiO_2/SiO_2 particles was rather complex. It was observed that the pzc value of all series of TiO_2/SiO_2 particles was lower than that of P-25, indicating that there were more acidic groups on the surface of TiO_2/SiO_2 particles.

3.2. Photoactivity of TiO_2/SiO_2 particles

3.2.1. UV-Vis spectra

An azo-dye acid orange 7 was chosen as a model pollutant due to its difficult to biodegradation and light degradation. The temporal evolution of the spectral changes taking place during the photodegradation of AO7 mediated by 31% TiO_2/SiO_2 particles under visible light irradiation was shown in Fig. 6. The electronic absorption spectrum of AO7 in water was characterized by four bands in the UV-Vis region. Two bands in visible region, with a major absorption band at 484 nm and a shoulder band at 430 nm, were due to the hydrazone form and azo form of AO7, respectively [23]. Two bands in the ultraviolet region located at 230 and 310 nm attributed to the benzene and naphthalene rings of AO7, respectively [24]. The extent of adsorption of AO7 (60 ppm) on TiO_2/SiO_2 particles (2 g/l) was ca. 45%, indicating the strong interaction between AO7 and TiO_2/SiO_2 particles. As observed in Fig. 6, the intensity of the 484 nm absorption band due to the chromophore decreased rapidly under visible light irradiation and almost disappeared after about 6 h, indicating the degradation of AO7 in the presence of 31% TiO_2/SiO_2 particles. Concomitantly, no new absorption band appeared in the UV-Vis region. This confirmed the photodegradation of AO7, i.e., the breakup of the chromophore responsible for the characteristic color of the dye, rather than its discoloration or bleaching. Moreover, the intensities of the absorption bands at 230 and 310 nm decreased rather slowly during the irradiation time, indicating that the intermediates formed during the photodegradation of the azo dye still contained benzoic- and naphthalene-type ring. After the total disappearance of the dye, the intensity of the band at 230 and 310 nm stopped to increase, indicating that the degradation of the dye was through the photosensitization way. The photodegradation of AO7 under visible light tended to follow pseudo-first-order kinetics in the presence of 31% TiO_2/SiO_2 particles, as shown in Fig. 6 (inset).

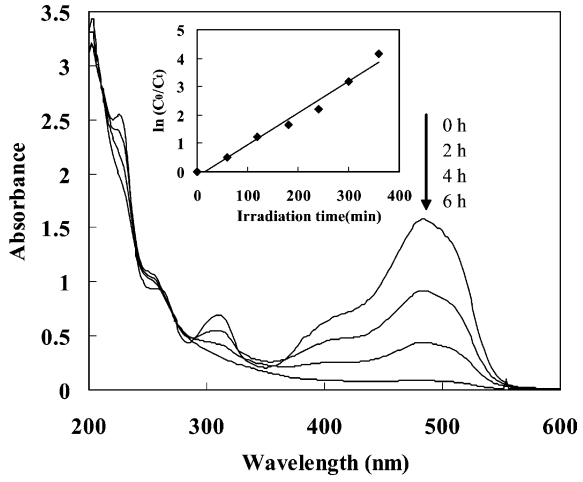

Fig. 6. UV-Vis spectral changes of AO7 (60 ppm, pH = 5.0) in aqueous 31% TiO_2/SiO_2 dispersions as a function of irradiation time. Inset: the plot $\ln(C_0/C_t)$ vs. irradiation time under the same conditions.

For comparison, blank experiments established that AO7 did not degrade in TiO_2/SiO_2 dispersion in the dark or when irradiated with visible light without photocatalysts. Therefore, we inferred from this that both visible light and TiO_2/SiO_2 particles were indispensable to the photodegradation of AO7. Moreover, visible light irradiation of AO7 in the presence of silica gel particles, substituted for TiO_2/SiO_2 particles, also caused no degradation of the dye, indicating the need for a semiconductor electron-transfer mediator.

It is clear from the above experimental results that AO7 undergoes the photodegradation process initiated by an electron injection into the conduction band of TiO_2 under visible light irradiation [25]. The potential for oxidation of the excited dye AO7 to the dye cationic radical ($E(AO7^*/AO7^{\bullet+}) = -1.24\,V$ versus NHE) [25] lies above the conduction band edge of TiO_2 ($E_{cb} = -0.5$ V versus NHE). Therefore, the occurrence of the interfacial electron transfer is thermodynamically feasible.

3.2.2. Effect of the calcination temperature

The effect of the calcination temperature on the photoactivity of 31% TiO_2/SiO_2 particles is shown in Fig. 7. It was observed that the apparent rate constant for the photodegradation of AO7 was decreased with increasing the calcination temperature, which was in consistent with the change of adsorption amount of AO7 and BET surface area of TiO_2/SiO_2 particles. When the calcination temperature increased from 300 to 400 °C, the photoactivity of TiO_2/SiO_2 particles was significantly reduced.

3.2.3. Effect of the TiO_2 loading

Fig. 8 shows that the apparent rate constant of TiO_2/SiO_2 particles for the photodegradation of AO7 changes with the TiO_2 loading. For the catalysts with low TiO_2 loading (<31%), the apparent rate constant was increased rapidly with increasing the TiO_2 loading. Since the photodegradation of dye pollutants only takes place on the surface of TiO_2 particles, the increase of the TiO_2 loading increased the surface coverage of TiO_2 on the silica gel, which led to

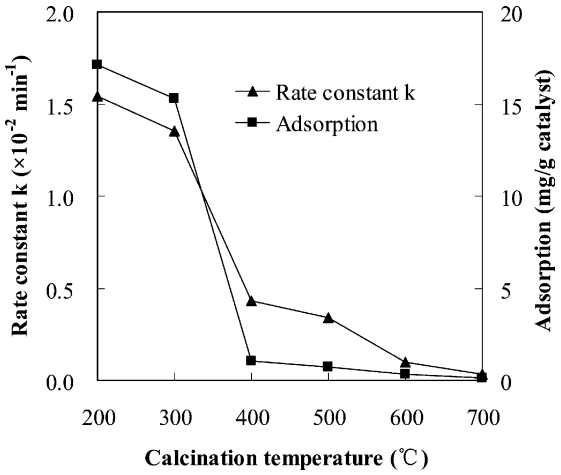

Fig. 7. Apparent rate constant and adsorption of 31% TiO_2/SiO_2 particles for the photodegradation of AO7 (40 ppm, pH = 5.0) under visible light irradiation as a function of the calcination temperature.

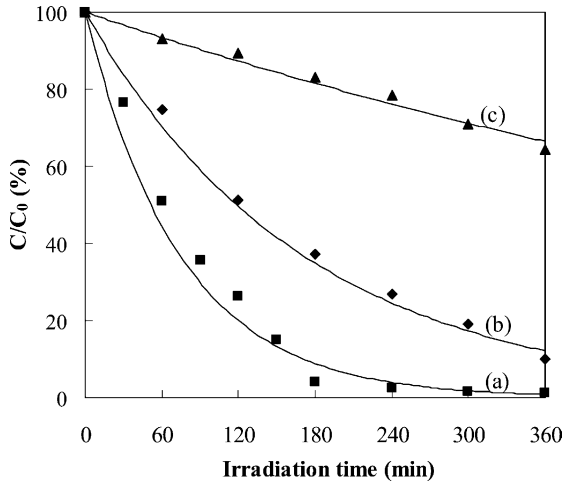

Fig. 9. Photodegradation of AO7 (40 ppm, pH = 5.0) in the presence of (a) 31% TiO_2/SiO_2; (b) P-25; and (c) TiO_2 (Shanghai) particles under visible light irradiation.

the enhancement of the rate of photodegradation of the dye. While for the catalysts with high TiO_2 loading (>31%), the apparent rate constant was increased slowly with increasing the TiO_2 loading, indicating that the rate-limiting step may be the supply of molecular oxygen to the catalyst surface under high TiO_2 loading. The efficiency of the photodegradation of AO7 under visible light irradiation is determined by the competition between forward electron injection and back electron transfer [23]. Under high TiO_2 loading, the high coverage of TiO_2 on the silica gel was significantly effective to accelerate the electron injection rate. However, the supply rate of molecular oxygen, which acts as an electron scavenger to avoid recombination of injected electron with $AO7^{\bullet+}$, was constant under experimental conditions. Therefore, the recombination rate of injected electrons with $AO7^{\bullet+}$ was also enhanced, thus, leading to the slow increase of the reaction rate constant under high TiO_2 loading.

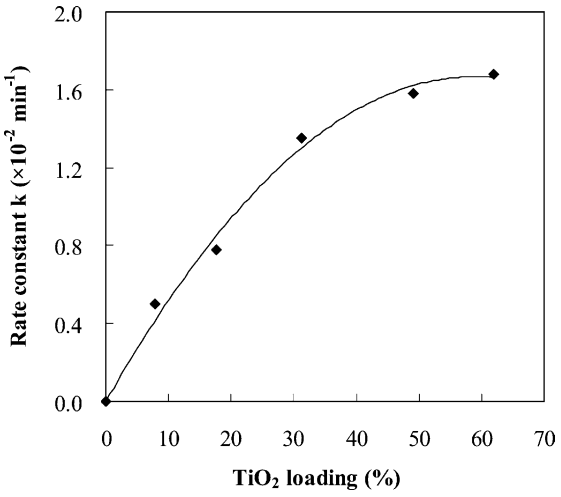

Fig. 8. Apparent rate constant of TiO_2/SiO_2 particles calcined at 300 °C for the photodegradation of AO7 (40 ppm, pH = 5.0) under visible light irradiation as a function of the TiO_2 loading.

3.2.4. Comparison with pure TiO_2

To compare the photoactivity of plain TiO_2 and TiO_2/SiO_2 particles, 2 g/l TiO_2 (Shanghai) and P-25 were used as reference catalyst. All the results are presented in Fig. 9. It was found that the kinetics of photodegradation for the dye all followed pseudo-order-kinetics. After 6 h of visible light irradiation, 99, 90 and 36% of the dye in an aqueous dispersion was degraded by TiO_2/SiO_2, P-25 and TiO_2 (Shanghai), respectively. It should be noted that TiO_2 only accounts for 31% mass of TiO_2/SiO_2 particles.

Since the preadsorption on the surface of TiO_2 particles is prerequisite for efficient photodegradation of dye pollutants under visible light irradiation [15], greater adsorption should enhance the degradation rate of AO7. Earlier studies [26] reported that adsorption of AO7 on the surface of TiO_2 occurs through a Lewis acid–base reaction, which implies the formation of an inner-sphere complex. The AO7 molecule is linked to three Ti^{IV} surface metallic cations through two oxygen atoms from the sulfonate group and the oxygen atom of the carbonyl group of the hydrazone tautomer. Therefore, the increase of the surface area of the catalyst will increase the site of Ti^{IV} surface metallic cations, resulting in the increase of adsorption of AO7 on the surface of the catalyst and the enhancement of the rate of electron transfer. As shown in Table 4, BET surface area of 31% TiO_2/SiO_2 particles was much higher than that of P-25 and TiO_2 (Shanghai) particles by 4.5 and 20.5 times, respectively. The adsorption of AO7 on the 31% TiO_2/SiO_2 particles was particularly strong, compared with pure TiO_2. The adsorption order of the three series catalysts was 31% TiO_2/SiO_2 > P-25 > TiO_2 (Shanghai), which was qualitatively consistent with the order of BET surface area. The photoactivity of the 31% TiO_2/SiO_2 particles determined

Table 4
Comparison of different catalysts for the photodegradation of AO7 under visible light irradiation[a]

Catalyst[b]	BET (m^2/g)	Adsorption (mg/g catalyst)	Rate constant (min^{-1})	r
31% TiO_2/SiO_2	225	15.3	0.0135	0.947
P-25	50	5.0	0.0059	0.981
TiO_2 (Shanghai)	11	0.2	0.0011	0.981

[a] Photocatalysts: 2 g/l; AO7: 40 ppm; irradiation time: 360 min.
[b] All photocatalysts were calcined at 300 °C for 2 h.

from the apparent rate constant was much higher than that of pure TiO_2. The visible light induced photodegradation rate of AO7 using 31% TiO_2/SiO_2 particles was faster than that using P-25 and TiO_2 (Shanghai) as photocatalyst by 2.3 and 12.3 times, respectively. The sequence of the photoactivity matched rather well with adsorption and BET surface area of the catalysts. The results confirmed that adsorption is significantly effective to enhance the rate of photodegradation of AO7 under visible light irradiation.

Moreover, TiO_2/SiO_2 particles had good sedimentation ability and could decant in a few minutes. Some sedimentation experiments carried out in the same experimental conditions showed that TiO_2/SiO_2 particles decanted from the suspension in 4 min, while P-25 and TiO_2 (Shanghai) particles did not decant after 24 h.

4. Conclusion

Silica gel supported catalysts (TiO_2/SiO_2) had been synthesized by using acid-catalyzed sol–gel method and characterized by different physical techniques. With increasing of the calcination temperature and the TiO_2 loading, the average crystallite size of TiO_2 increased, and BET surface area decreased linearly. The rutile phase of TiO_2 was not formed at high calcination temperature, indicating the good thermal stability of TiO_2/SiO_2 particles. The photoactivity of TiO_2/SiO_2 particles increased with increasing the TiO_2 loading and with decreasing the calcination temperature.

For the degradation of AO7 under visible light irradiation, the photoactivity of TiO_2/SiO_2 particles determined from the apparent rate constant was much better than that of pure TiO_2. The photodegradation rate of AO7 using 31% TiO_2/SiO_2 particles was faster than that using P-25 and TiO_2 (Shanghai) as photocatalyst by 2.3 and 12.3 times, respectively. The high surface area and great adsorption of TiO_2/SiO_2 particles facilitated electron injection so as to significant increased the rate of photodegradation of AO7. Moreover, The TiO_2/SiO_2 particles had good sedimentation ability.

Acknowledgements

The authors wish to express their appreciation to Prof. G. Lv and Prof. X. Jiang for their help in XRD and BET measurement.

References

[1] E.J. Weber, R.L. Adams, Environ. Sci. Technol. 29 (1995) 1163.
[2] H. Zollinger, Color Chemistry: Synthesis, Properties and Applications of Organic Dye and Pigments, VCH Publishers, New York, 1983.
[3] I. Arslan, I.A. Balcioglu, D.W. Bahnemann, Dyes Pigments 47 (2000) 207.
[4] K. Tanaka, K. Padermpole, T. Hisanaga, Water Res. 34 (2000) 327.
[5] K.-T. Chung, C.E. Cerniglia, Mutat. Res. 277 (1992) 201.
[6] F. Herrera, A. Lopez, G. Mascolo, P. Albers, J. Kiwi, Water Res. 35 (2001) 750.
[7] P. Cooper, J. Soc. Dyers Colour 109 (1993) 97.
[8] M.A. Fox, M.T. Dulay, Chem. Rev. 93 (1993) 341.
[9] R.W. Matthews, Water Res. 25 (1991) 1169.
[10] S. Sakthivel, M.V. Shankar, M. Palanichamy, B. Arabindoo, V. Murugesan, J. Photochem. Photobiol. A: Chem. 148 (2002) 153.
[11] T. Watanable, T. Takizawa, K. Honda, J. Phys. Chem. 81 (1977) 1845.
[12] P.V. Kamat, M.A. Fox, Chem. Phys. Lett. 102 (1983) 379.
[13] P.V. Kamat, J. Phys. Chem. 93 (1989) 859.
[14] B. Patrick, P.V. Kamat, J. Phys. Chem. 96 (1992) 1423.
[15] J. Zhao, T. Wu, K. Wu, K. Oikawa, H. Hidaka, N. Serpone, Environ. Sci. Technol. 32 (1998) 2394.
[16] H. Chun, Y. Wang, H. Tang, Appl. Catal. B: Environ. 30 (2001) 277.
[17] S. Subramanian, J.S. Noh, J.A. Schwarz, J. Catal. 114 (1988) 433.
[18] J.S. Noh, J.A. Schwarz, J. Colloid Interface Sci. 130 (1989) 157.
[19] A.L. Pruden, D.F. Ollis, J. Catal. 82 (1983) 404.
[20] D.F. Ollis, Environ. Sci. Technol. 19 (1985) 480.
[21] K.Y. Jung, S.B. Park, Appl. Catal. B: Environ. 25 (2000) 249.
[22] C. Kormann, D.W. Bahnemann, M.R. Hoffmann, Environ. Sci. Technol. 25 (1991) 494.
[23] C. Bauer, P. Jacques, A. Kalt, J. Photochem. Photobiol. A: Chem. 140 (2001) 87.
[24] W. Feng, D. Nansheng, H. Helin, Chemosphere 41 (2000) 1233.
[25] K. Vinodgopal, D.E. Winkoop, P.V. Kamat, Environ. Sci. Technol. 30 (1996) 1660.
[26] C. Bauer, P. Jacques, A. Kalt, Chem. Phys. Lett. 307 (1999) 397.